Smart Structures and Systems, *Vol. 13, No. 2 (2014) 319-341*
DOI: http://dx.doi.org/10.12989/sss.2014.13.2.319

Family of smart tuned mass dampers with variable frequency under harmonic excitations and ground motions: closed-form evaluation

C. Sun[1], S. Nagarajaiah[*1,2] and A.J. Dick[2]

[1]*Department of Civil and Environmental Engineering, Rice University, Houston, Texas 77005, USA*
[2] *Department of Mechanical Engineering and Materials Science, Rice University, Houston, Texas 77005, USA*

(Received December 19, 2013, Revised January 7, 2014, Accepted January 9, 2014)

Abstract. A family of smart tuned mass dampers (STMDs) with variable frequency and damping properties is analyzed under harmonic excitations and ground motions. Two types of STMDs are studied: one is realized by a semi-active independently variable stiffness (SAIVS) device and the other is realized by a pendulum with an adjustable length. Based on the feedback signal, the angle of the SAIVS device or the length of the pendulum is adjusted by using a servomotor such that the frequency of the STMD matches the dominant excitation frequency in real-time. Closed-form solutions are derived for the two types of STMDs under harmonic excitations and ground motions. Results indicate that a small damping ratio (zero damping is the best theoretically) and an appropriate mass ratio can produce significant reduction when compared to the case with no tuned mass damper. Experiments are conducted to verify the theoretical result of the smart pendulum TMD (SPTMD). Frequency tuning of the SPTMD is implemented through tracking and analyzing the signal of the excitation using a short time Fourier transformation (STFT) based control algorithm. It is found that the theoretical model can predict the structural responses well. Both the SAIVS STMD and the SPTMD can significantly attenuate the structural responses and outperform the conventional passive TMDs.

Keywords: smart tuned mass dampers (STMDs); harmonic excitation and ground motion; frequency tracking; closed-form solutions; experimental verification

1. Introduction

In the community of structural vibration control, Tuned Mass Dampers (TMDs), as effective approaches to reduce structural dynamic responses, are well understood and have been deployed in many buildings and bridges. When tuned to the fundamental frequency of the structure, TMDs can minimize the structural response at its resonant frequency. The idea of the TMD was proposed and patented by Frahm in 1911. Then in 1928, Ormondroyd and Den Hartog theoretically investigated the TMD in an undamped single-degree-of-freedom (SDOF) system subjected to harmonic loadings (Ormondroyd and Den Hartog 1928). Optimum design parameters for TMDs are presented in the textbook (Den Hartog 1956). Since then, TMDs have been widely studied and

*Corresponding author, Professor, E-mail: satish.nagarajaiah@rice.edu

http://www.techno-press.org/?journal=sss&subpage=8 ISSN: 1738-1584 (Print), 1738-1991 (Online)

many new types of TMDs have been developed and evaluated (Housner *et al*. 1997, Spencer and Nagarajaiah 2003). However, the narrow effective bandwidth of TMDs in the frequency domain can cause the malfunction of TMDs when the natural frequency of the primary structure shifts due to structural degradation or other reasons.

In order to overcome the drawbacks of conventional TMDs, researchers proposed Semi-active Tuned Mass Dampers (STMDs) which are realized by variable damping or stiffness devices. Since the 1980s, STMDs have been studied and shown more effective than their equivalent passive counterparts and more reliable than their equivalent active counterparts. In addition, no stability issues would arise in the case of STMDs since they do not apply direct forces to structures (Housner *et al*. 1997). Hrovat *et al.* evaluated the performance of an STMD in reducing wind-induced vibrations of tall buildings (Hrovat *et al*. 1983). They varied the damping ratio of the STMD based on the feedback and the associated control algorithm. Their findings showed that the STMD could provide a reduction effect comparable to that of its equivalent active counterparts and outperform its equivalent passive counterparts. Abe and Igusa established closed-form solutions for the optimum initial displacement and variable damping ratio of an STMD to control transient responses (Abe and Igusa 1996). Abe further examined the performance of the STMD to protect civil structures during earthquakes (Abe 1996). Their findings indicated that the STMD with an optimum initial displacement and variable damping ratio can produce better reduction than the passive TMDs.

Since then, many variable damping devices have been developed and used in STMDs, including the magnetorheological (MR) dampers, the variable orifice dampers and the electrorheological (ER) dampers (Spencer and Nagarajaiah 2003). Meanwhile, the active variable stiffness (AVS) system was pioneered by Kobori and implemented in a full-scale structure in Tokyo, Japan (Kobori *et al*. 1993). It was found that the AVS system could influence the structure into a non-resonant state against earthquake excitations, thereby suppressing the structural responses. However, it was observed in (Yamada and Kobori 1995) that the abrupt switching of the system could influence its performance in controlling vibrations.

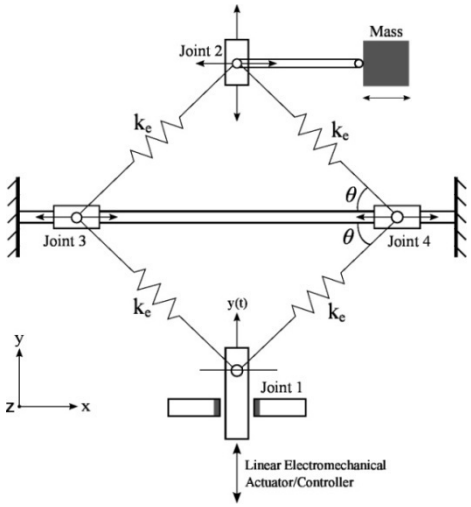

Fig. 1 Semi-Active and Independently Variable Stiffness (SAIVS) device and STMD (Nagarajaiah 2000)

In comparison, Nagarajaiah and Mate (1998), Nagarajaiah (2000) developed a semi-active continuously and independently variable-stiffness (SAIVS) device as shown in Fig. 1. Based on the SAIVS device, a new type of smart Tuned Mass Damper (STMD) with variable stiffness and damping property is proposed and examined (Varadarajan and Nagarajaiah 2004, Nagarajaiah and Varadarajan 2005, Nagarajaiah and Sonmez 2007, Nagarajaiah 2009, Sun and Nagarajaiah 2013).

It was found that the SAIVS device can provide reliably and smoothly variable stiffness such that the frequency of the STMD can be tuned in real-time. The capability of the STMD to attenuate structural responses was validated analytically and experimentally for both stationary and non-stationary excitations. The authors found that the SAIVS STMD performs comparably to an active TMD but requires an order of magnitude less power. Recently, Sun *et al.* evaluated the performance of the SAIVS STMD in parallel with a nonlinear TMD (NTMD) to control a Düffing system (Sun *et al*. 2013). Their results indicated that the combination of an STMD and an NTMD in parallel can effectively attenuate the structural responses: both the transient and the steady-state responses. Eason *et al.* studied the behavior of the SAIVS STMD and an NTMD in series to control a linear primary structure (Eason *et al*. 2013). They found that an STMD with a mass four orders of magnitude smaller than the primary structure is able to greatly reduce the amplitude of the structural response.

In addition to the conventional TMDs, the pendulum TMD (PTMD) consisting of a cable and a mass suspended at the top part of a building has received popularity in the community of vibration control in recent years. Mehdi *et al.* used the PTMD to control excessive floor vibrations due to human movements (Yamada *et al*. 2006). Their results indicated that a properly-tuned PTMD can effectively control the floor vibrations while an off-tuned PTMD may not function effectively. In order to overcome the off-tuning of PTMD, Nagaragaiah proposed the concept of an adaptive-length pendulum TMD (APL-PTMD) (Nagarajaiah 2009). It was shown experimentally that the APL-PTMD can significantly reduce the structural responses and outperforms its equivalent passive counterpart. Recently, Sun *et al.* studied the performance of an adaptive pendulum TMD (APTMD) in parallel with a nonlinear TMD used to attenuate the responses of a primary a Düffing system (Sun *et al*. 2013). The authors demonstrated that the APTMD can effectively attenuate the hazardous high amplitude detached resonance of the primary structure (Eason *et al*. 2013). However, closed-form solutions of SAIVS-STMD and APL-PTMD are still needed to study a more general family/class of the two types of STMD, which is the focus of this study.

Motivated by the work described above, two types of smart tuned mass damper (STMD) with variable frequency properties are studied theoretically and experimentally in the present study. The two types of STMD are realized by the semi-active independently variable stiffness (SAIVS) device and a pendulum with adjustable length. The performance of both the SAIVS STMD and the smart pendulum TMD (SPTMD) is analyzed. Equations of motion of the dynamic system are established. Closed-form solutions of the structure STMD (or SPTMD) two degrees-of-freedom system which is essentially a time variant system are derived, providing insight into the dynamic system. In the case of SPTMD, an approximate simplification is used to linearize the essentially nonlinear equations, thereby making it solvable directly. It is shown that the solution is appropriate when excitation and ground motion amplitude is relatively small. Experimental data with respect to the SPTMD is presented to verify the theoretical model showing that the simplified linear model can predict the performance of the SPTMD well.

The paper is structured as follows. The next section describes two configurations of the dynamic system coupled with an STMD and an SPTMD. Section 3 presents the relevant equations

of motion of the dynamic system and the solutions to the equations are derived. The performance of the STMD and the SPTMD under harmonic excitations and ground motions are presented in Section 4. Section 5 presents the experimental verification of the SPTMD. Concluding remarks are discussed in the final section.

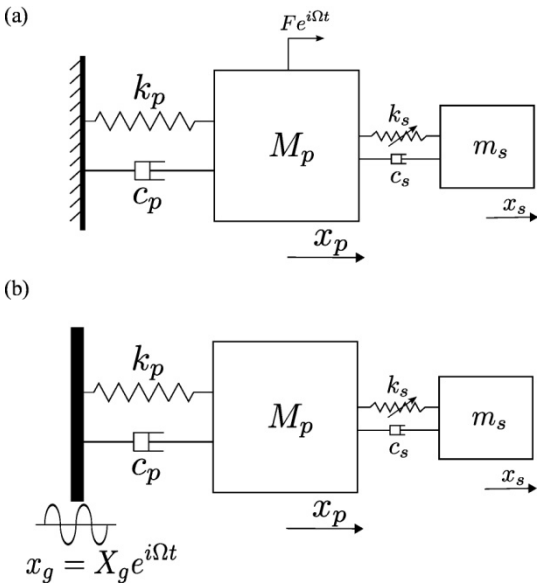

Fig. 2 Illustration of the dynamic system coupled with an STMD under harmonic excitation (a) and ground motion (b)

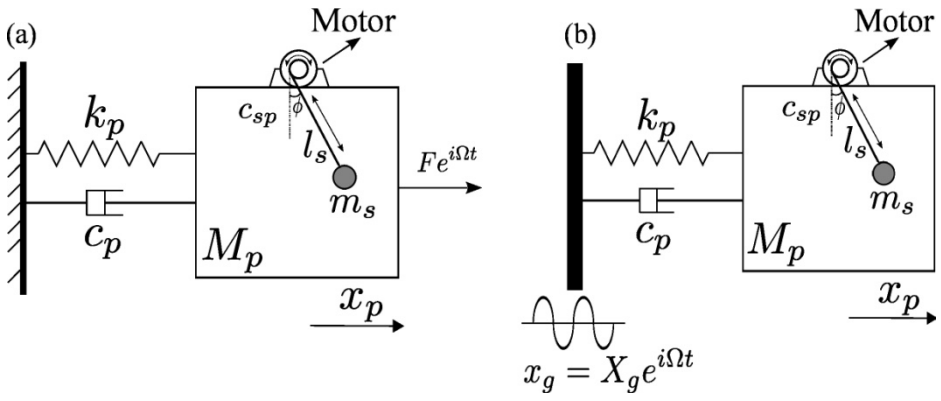

Fig. 3 Illustration of the smart pendulum tuned mass damper and the SDOF

2. Description of the models

In this section, the configuration of a single degree-of-freedom (SDOF) primary structure with two types of STMD, i.e., the SAIVS STMD and the smart pendulum TMD (SPTMD), are illustrated and described in the following subsections respectively.

2.1. Configuration of the primary system with an SAIVS STMD

The dynamic system consisting of a linear structure and a SAIVS STMD (STMD) excited harmonically are presented in Fig. 2 where the structure is subjected to harmonic loadings in Fig. 2(a) and to harmonic ground motions in Fig. 2(b). The natural frequency of the STMD is controlled through varying the angle θ of the SAIVS device by using a linear electro-mechanical motor.

2.2. Configuration of the primary system with a pendulum STMD

The dynamic system consisting of a linear structure and a pendulum STMD (SPTMD) excited harmonically are presented in Fig. 3 where the structure is subjected to harmonic excitations in Fig. 3(a) and to harmonic ground motions in Fig. 3(b). The natural frequency of the SPTMD is controlled through varying the length l_s of the pendulum using a linear electro-mechanical motor.

It is noted that the damping coefficient of the SAIVS-STMD in Fig. 2 is denoted as c_s whose unit is $N \cdot s/m$ and the damping coefficient of the SPTMD shown in Fig. 3 is denoted as c_{sp} whose unit is $N \cdot s/m$.

3. Closed-form solutions of the dynamic system with STMD and SPTMD

In this section, the closed-form solutions of the dynamic system with STMD and SPTMD are derived. In order to perform this analysis, a complex form is assumed for the excitation, the ground motion, and the response terms. The harmonic loading is assumed to take the form $f = Fe^{i\Omega t}$ where F is the forcing amplitude and Ω is the frequency; the ground motion is $x_g = X_g e^{i\Omega t}$ where X_g and Ω are the ground motion amplitude and frequency, respectively. For the sake of clarification, the subscript *s* is used to denote the result in the case of STMD and the subscript *sp* is used in the case of the SPTMD. The STMD case is referred as Model I and the SPTMD is referred as Model II for convenience.

3.1 Dynamic system with STMD

This section presents the equations of motion of Model I. Solutions are then derived for the two models under both harmonic excitation and harmonic ground motion.

3.1.1 Under harmonic excitations

The equations of motion of Model I under harmonic loading as shown in Fig. 2(a) are derived

using the Euler-Lagrange equation and shown in Eq. (1). Details regarding the derivation of the equation are illustrated in the Appendix.

$$\begin{aligned} M_p\ddot{x}_p + c_p\dot{x}_p + k_p x_p + c_s(\dot{x}_p - \dot{x}_s) + k_s(x_p - x_s) &= Fe^{i\Omega t} \\ m_s\ddot{x}_s + c_s(\dot{x}_s - \dot{x}_p) + k_s(x_s - x_p) &= 0 \end{aligned} \tag{1}$$

where M_p is a variable representing the mass of the primary structure, and m_s is the mass of the STMD. Variables c_p, c_s denote the viscous damping coefficient of the primary structure and the STMD. Stiffness coefficients corresponding to the primary structure and the STMD are k_p and k_s respectively. Variables x_p and x_s denote the position of the two degree of freedom system. An over-dot ($\dot{}$) indicates the derivative with respect to time.

In order to express the equations of motion in terms of the design parameters, Eqs. (2) and (3) are utilized.

$$\omega_p = \sqrt{\frac{k_p}{M_p}}, \quad \omega_s = \sqrt{\frac{k_s}{m_s}}, \quad \Omega_s = \frac{\omega_s}{\omega_p}, \quad \zeta_p = \frac{c_p}{2M_p\omega_p}, \quad \zeta_s = \frac{c_s}{2m_s\omega_s}, \tag{2}$$

$$\varepsilon_s = \frac{m_s}{M_p}, \quad \omega = \frac{\Omega}{\omega_p}, \quad X_{pst} = \frac{F}{k_p}, \quad \tau = \omega_p t. \tag{3}$$

Non-dimensionalizing Eq. (1) with respect to time results in

$$\begin{aligned} \ddot{x}_p + 2\zeta_p\dot{x}_p + x_p + 2\varepsilon_s\Omega_s\zeta_s(\dot{x}_p - \dot{x}_s) + \varepsilon_s\Omega_s^2(x_p - x_s) &= X_{pst}e^{i\omega\tau}, \\ \ddot{x}_s + 2\zeta_s\Omega_s(\dot{x}_s - \dot{x}_p) + \Omega_s^2(x_s - x_p) &= 0 \end{aligned} \tag{4}$$

The general forms of the steady-state solutions of the dynamical system can be written as

$$x_p = A_p e^{i\omega\tau}, \quad x_s = A_s e^{i\omega\tau} \tag{5}$$

where parameters A_p and A_s are complex numbers which contain the amplitude and phase angle of the responses.

Substituting Eq. (5) into Eq. (4) and rewriting the equation in matrix form yields

$$\begin{bmatrix} -\omega^2 + 2i\omega\zeta_p + 2i\varepsilon_s\omega\Omega_s\zeta_s + \varepsilon_s\Omega_s^2 + 1 & -2i\varepsilon_s\omega\Omega_s\zeta_s - \varepsilon_s\Omega_s^2 \\ -2i\omega\Omega_s\zeta_s - \Omega_s^2 & -\omega^2 + 2i\omega\zeta_s\Omega_s + \Omega_s^2 \end{bmatrix} \begin{Bmatrix} A_p \\ A_s \end{Bmatrix} = \begin{Bmatrix} X_{pst} \\ 0 \end{Bmatrix} \tag{6}$$

Solving Eq. (6) for A_p and A_s yields the transfer functions

$$H_p(i\omega) = \frac{A_p}{X_{pst}} = \frac{A_{22}}{D}, \qquad H_s(i\omega) = \frac{A_s}{X_{pst}} = \frac{A_{21}}{D} \tag{7}$$

where

$$A_{22} = -\omega^2 + 2i\omega\Omega_s\zeta_s + \Omega_s^2,$$

$$A_{21} = 2i\omega\Omega_s\zeta_s + \Omega_s^2,$$

$$D = (-\omega^2 + \varepsilon_s\Omega_s^2 + 2i\omega\zeta_p + 2i\varepsilon_s\omega\Omega_s\zeta_s + 1)(-\omega^2 + \Omega_s^2 + 2i\omega\Omega_s\zeta_s) - (\Omega_s^2 + 2\omega\Omega_s\zeta_s)(\varepsilon_s\Omega_s^2 + 2\varepsilon_s\omega\Omega_s\zeta_s)$$

Separating the real and imaginary parts of H_p and H_s gives

$$\begin{aligned} H_p &= c_p + id_p, \\ H_s &= c_s + id_s \end{aligned} \tag{8}$$

where c_p, c_s, d_p, d_s are the real parts and the imaginary parts of H_p, H_s and the associated formulas are listed in the Appendix.

Based on Eq. (8), the magnitude and phase angle of H_p and H_s are derived as

$$|H_p| = \sqrt{c_p^2 + d_p^2}, \quad |H_s| = \sqrt{c_s^2 + d_s^2} \tag{9}$$

$$\theta_p = arctan\left(-\frac{d_p}{c_p}\right), \quad \theta_s = arctan\left(-\frac{d_s}{c_s}\right), \quad \theta_r = \left| arctan\left(\frac{d_p c_s - c_p d_s}{d_p d_s + c_p c_s}\right)\right| \tag{10}$$

where θ_p, θ_s and θ_r are the phase angles of the primary structure, the STMD, and the phase difference between the structure and the STMD.

Multiplying the steady-state response of the displacement by ω^2 yields the transfer functions of the acceleration listed as follows

$$\begin{aligned} |H_{pacce}| &= \omega^2 \sqrt{c_p^2 + d_p^2}, \\ |H_{sacce}| &= \omega^2 \sqrt{c_s^2 + d_s^2} \end{aligned} \tag{11}$$

3.1.2 Under ground motions

Similarly, the equations of motion of Model I under harmonic ground motions are derived as

$$\begin{aligned} M_p \ddot{x}_{rp} + c_p \dot{x}_{rp} + k_p x_{rp} + c_s(\dot{x}_{rp} - \dot{x}_s) + k_s(x_{rp} - x_{rs}) &= -M_p \ddot{x}_g, \\ m_s \ddot{x}_{rs} + c_s(\dot{x}_{rs} - \dot{x}_{rp}) + k_s(x_s - x_{rp}) &= -m_s \ddot{x}_g \end{aligned} \tag{12}$$

where x_{rp} and x_{rs} denote the relative displacement of the primary structure and the STMD to the base.

Non-dimensionalizing Eq. (12) produces

$$\begin{aligned} \ddot{x}_p + 2\zeta_p \dot{x}_p + x_p + 2\varepsilon_s \Omega_s \zeta_s (\dot{x}_p - \dot{x}_s) + \varepsilon_s \Omega_s^2 (x_p - x_s) &= -\omega^2 X_g e^{i\omega\tau}, \\ \ddot{x}_s + 2\zeta_s \Omega_s (\dot{x}_s - \dot{x}_p) + \Omega_s^2 (x_s - x_p) &= -\omega^2 X_g e^{i\omega\tau} \end{aligned} \tag{13}$$

The general forms of the steady-state solutions of Eq. (13) can be written as

$$\begin{aligned} x_{rp} &= A_{rp} e^{i\omega\tau}, \\ x_{rs} &= A_{rs} e^{i\omega\tau} \end{aligned} \tag{14}$$

Substituting Eq. (14) into Eq. (13) yields the transfer functions listed in the following equations

$$H_{pg} = \frac{A_{rp}}{X_g} = \frac{\omega^2 (A_{12} - A_{22})}{D}, \qquad A_{sg} = \frac{A_{rs}}{X_g} = \frac{\omega^2 (A_{21} - A_{11})}{D} \tag{15}$$

$$H_{pgacce} = \frac{\omega^2 (A_{12} - A_{22})}{D} + 1, \qquad A_{sgacce} = \frac{\omega^2 (A_{21} - A_{11})}{D} + 1 \tag{16}$$

where H_{pg}, H_{sg} denote the relative displacement transfer function, and H_{pgacce}, H_{sgacce} denote the absolute acceleration transfer function corresponding to ground motions; $A_{11} = -\omega^2 + 2i\omega\zeta_p + 2i\varepsilon_s\omega\Omega_s\zeta_s + \varepsilon_s\Omega_s^2 + 1$, $A_{12} = -2i\varepsilon_s\omega\Omega_s\zeta_s - \varepsilon_s\Omega_s^2$, $A_{22} = -\omega^2 + 2i\omega\Omega_s\zeta_s + \Omega_s^2$

3.2. Dynamical system with SPTMD

3.2.1 Under harmonic excitations

The equations of motion of Model II under harmonic excitation are shown in Eq. (17). Details of the derivation of the equations are illustrated in the Appendix.

$$\begin{aligned} (M_p + m_s)\ddot{x}_p + c_p\dot{x}_p + k_p x_p + m_s l_s(\ddot{\phi}cos\phi - \dot{\phi}^2 sin\phi) = Fe^{i\omega t}, \\ m_s l_s cos\phi\ddot{x}_p + m_s l_s^2\ddot{\phi} + c_{sp}\dot{\phi} + m_s g l_s sin\phi = 0 \end{aligned} \tag{17}$$

In addition to Eqs. (2) and (3), the following equations are utilized to define the equations of motion in terms of the design parameters for Model II.

$$\omega_{sp} = \sqrt{\frac{g}{l_s}}, \quad \Omega_{sp} = \frac{\omega_{sp}}{\omega_p}, \quad \zeta_{sp} = \frac{c_{sp}}{2m_s l_s^2 \omega_{sp}} \tag{18}$$

where g is the acceleration due to gravity.

Non-dimensionalizing Eq. (17) using Eqs. (2) and (3) and Eq. (18) yields

$$\begin{aligned} (1+\varepsilon_s)\ddot{x}_p + 2\zeta_p\dot{x}_p + x_p + \varepsilon_s l_s(\ddot{\phi}cos\phi - \dot{\phi}^2 sin\phi) = X_{pst}e^{i\omega\tau}, \\ \frac{cos\phi}{l_s}\ddot{x}_p + \ddot{\phi} + 2\zeta_s\omega_{sp}\dot{\phi} + \omega_{sp}^2 sin\phi = 0 \end{aligned} \tag{19}$$

When the excitation amplitude F is small, the response of the system will be small, i.e., $0 < \phi \ll 1$. Then the nonlinear term $\dot{\phi}^2 sin\phi$ in Eq. (19) is small and thus can be neglected; in addition, $sin\phi \approx \phi$, and $cos\phi \approx 1$. Therefore, the original nonlinear ordinary differential equation Eq. (19) becomes linear ODEs which can be solved directly.

The general form of the steady-state solutions of Eq. (19) can be written as

$$\begin{aligned} x_p = A_{sp}e^{i\omega\tau}, \\ \phi = A_{ss}e^{i\omega\tau} \end{aligned} \tag{20}$$

where the subscripts *sp* and *ss* denote the primary structure and the pendulum in Model II, respectively.

Substituting Eq. (20) into Eq. (19) and rewriting the equation in matrix form yields

$$\begin{bmatrix} -(1+\varepsilon_s)\omega^2 + 2i\omega\zeta_p + 1 & -\varepsilon_s l_s\omega^2 \\ -\omega^2 / l_s & -\omega^2 + 2i\omega\zeta_s\Omega_s + \Omega_s^2 \end{bmatrix} \begin{Bmatrix} A_{sp} \\ A_{ss} \end{Bmatrix} = \begin{Bmatrix} X_{pst} \\ 0 \end{Bmatrix} \tag{21}$$

Solving Eq. (21) for A_{sp} and A_{ss} and the transfer functions are presented as

$$H_{sp}(i\omega)=\frac{-\omega^2+2i\omega\Omega_s\zeta_s+\Omega_s^2}{[-(1+\varepsilon_s)\omega^2+2i\omega\zeta_p+1][-\omega^2+2i\zeta_s\Omega_s\omega+\Omega_s^2]-\varepsilon_s\omega^4} \tag{22}$$

$$H_{ss}(i\omega)=\frac{l_s\varepsilon_s\omega^2}{[-(1+\varepsilon_s)\omega^2+2i\omega\zeta_p+1][-\omega^2+2i\zeta_s\Omega_s\omega+\Omega_s^2]-\varepsilon_s\omega^4} \tag{23}$$

where $H(i\omega)_{sp}$ and $H(i\omega)_{ss}$ are the transfer functions of the primary structure and the smart pendulum TMD, respectively.

Based on Eqs. (22) and (23), the acceleration transfer functions are obtained and shown as

$$H_{spacce}(i\omega)=\frac{\omega^4-2i\omega^3\Omega_s\zeta_s-\omega^2\Omega_s^2}{[-(1+\varepsilon_s)\omega^2+2i\omega\zeta_p+1][-\omega^2+2i\zeta_s\Omega_s\omega+\Omega_s^2]-\varepsilon_s\omega^4} \tag{24}$$

$$H_{ssacce}(i\omega)=\frac{-l_s\varepsilon_s\omega^4}{[-(1+\varepsilon_s)\omega^2+2i\omega\zeta_p+1][-\omega^2+2i\zeta_s\Omega_s\omega+\Omega_s^2]-\varepsilon_s\omega^4} \tag{25}$$

where the subscript *space* and *ssacce* refer to acceleration of the primary structure and the smart pendulum TMD.

3.2.2 Solution of the system under harmonic ground motions

Similarly, the equation of motion of Model II under ground motion x_g as shown in Fig. 2(b) is derived as

$$\begin{aligned}(M_p+m_s)\ddot{x}_{rp}+c_p\dot{x}_{rp}+k_px_{rp}+m_sl_s(\ddot{\phi}cos\phi-\dot{\phi}^2sin\phi)&=-(M_p+m_s)\ddot{x}_g,\\ m_sl_scos\phi\ddot{x}_{rp}+m_sl_s^2\ddot{\phi}+c_s\dot{\phi}+m_sgl_ssin\phi&=-m_sl_scos\phi\ddot{x}_g\end{aligned} \tag{26}$$

where x_{rp} is the relative displacement of the primary structure to the base.

By using the Eqs. (2) and (3) and Eq. (18), Eq. (26) can be non-dimensionalized as

$$\begin{aligned}(1+\varepsilon_s)\ddot{x}_{rp}+2\zeta_p\dot{x}_{rp}+x_{rp}+\varepsilon_sl_s(\ddot{\phi}\ cos\ \phi-\dot{\phi}^2sin\ \phi)&=-(1+\varepsilon_s)\ddot{x}_g(\tau),\\ \frac{cos\ \phi}{l_s}\ddot{x}_{rp}+\ddot{\phi}+2\zeta_s\omega_{sp}\dot{\phi}+\omega_{sp}^2sin\ \phi&=-\frac{cos\ \phi}{l_s}\ddot{x}_g(\tau)\end{aligned} \tag{27}$$

Based on the small angle approximation: $\dot{\phi}^2sin\phi\approx 0,\ sin\phi\approx\phi,\ cos\phi\approx 1,$ Eq. (27) can be linearizd and solved directly. The general forms of the steady-state solutions of Eq. (27) are written as

$$\begin{aligned}x_{rp}&=A_{sp}e^{i\omega\tau},\\ \phi&=A_{ss}e^{i\omega\tau}\end{aligned} \tag{28}$$

Substituting Eq. (28) into Eq. (27) and solving for A_{sp} and A_{ss} yields the transfer functions of the dynamic system under ground motions

$$H_{spg}(i\omega)=\frac{\omega^2[-\omega^2+2i(1+\varepsilon_s)\omega\Omega_s\zeta_s+(1+\varepsilon_s)\Omega_s^2]}{[-(1+\varepsilon_s)\omega^2+2i\omega\zeta_p+1][-\omega^2+2i\zeta_s\Omega_s\omega+\Omega_s^2]-\varepsilon_s\omega^4} \tag{29}$$

$$H_{ssg}(i\omega)=\frac{\omega^2(2i\omega\zeta_p+1)}{l_s\{[-(1+\varepsilon_s)\omega^2+2i\omega\zeta_p+1][-\omega^2+2i\zeta_s\Omega_s\omega+\Omega_s^2]-\varepsilon_s\omega^4\}} \tag{30}$$

$$H_{spgacce}(i\omega)=\frac{\omega^2[-\omega^2+2i(1+\varepsilon_s)\omega\Omega_s\zeta_s+(1+\varepsilon_s)\Omega_s^2]}{[-(1+\varepsilon_s)\omega^2+2i\omega\zeta_p+1][-\omega^2+2i\zeta_s\Omega_s\omega+\Omega_s^2]-\varepsilon_s\omega^4}+1 \tag{31}$$

$$H_{ssgacce}(i\omega)=\frac{\omega^4(2i\omega\zeta_p+1)}{l_s\{[-(1+\varepsilon_s)\omega^2+2i\omega\zeta_p+1][-\omega^2+2i\zeta_s\Omega_s\omega+\Omega_s^2]-\varepsilon_s\omega^4\}}+1 \tag{32}$$

where H_{spg} and H_{ssg} denote the relative displacement transfer functions, $H_{spgacce}$ and $H_{ssgacce}$ denote the absolute acceleration transfer functions corresponding to the ground motion.

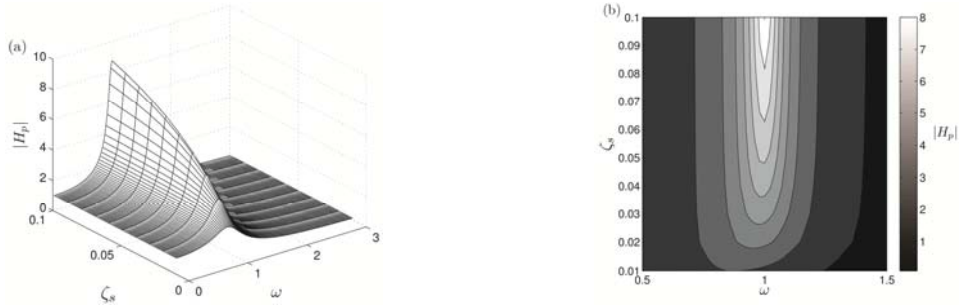

Fig. 4 Frequency response with various damping ratios under harmonic excitations: (a) response surface and (b) contour of the response surface. Mass ratio $\dot{\alpha}_s = 1\%$.

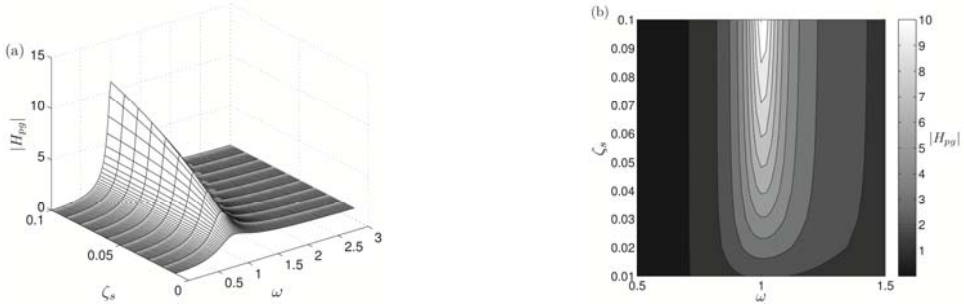

Fig. 5 Frequency response with various damping ratios under ground motions: (a) response surface and (b) contour of the response surface. Mass ratio $\dot{\alpha}_s = 1\%$

4. Results of the dynamic system with STMD/SPTMD

The closed-form results of the structural response with respect to both the STMD and SPTMD are presented in this section. An important parameter when studying these systems is the damping ratio of the structure. The typical damping ratio values for structures are in the range of

$[0.01 \quad 0.05]$, see (Newmark and Hall 1982). In the present study, $\zeta_p = 0.02$ is adopted for the primary structure.

4.1. Results of the SAIVS STMD

In order to absorb the energy of the primary structure effectively, two strategies are often used to tune the frequency of an STMD (Nagarajaiah 2009). The first is to tune the STMD such that its fundamental frequency matches the dominant response frequency of the primary structure, typically near its first natural frequency. The second is to tune the natural frequency of an STMD to the dominant excitation frequency, i.e., $\omega_s = \Omega$. In the present study, the second tuning method is used and thus the natural frequency of the STMD/SPTMD is time dependent. The control procedure can be described as follows: first, the excitation signal is tracked and analyzed to provide the dominant frequency of the excitation; then the natural frequency of the STMD/SPTMD is tuned to match the dominant excitation frequency by means of changing the angle of the SAIVS device in the case of the SAIVS STMD or adjusting the length of the pendulum in the case of the SPTMD. Because the tracking and analyzing with respect to the signal is not the focus of the current study, details are not illustrated here. In the case of the SAIVS STMD, the damping coefficient c_s is tuned in terms of ω_s such that the damping ratio ζ_s remains constant; similarly, the damping coefficient c_{sp} is tuned in terms of ω_{sp} such that the damping ratio ζ_{sp} remains constant. In this section, the reduction effect with respect to different damping ratios and mass ratios are presented. In addition, the sensitivity of the tuning frequency ratio ω_s / Ω is analyzed with various damping ratios and mass ratios.

4.1.1 Study on STMD damping ratio

The frequency response surface and the associated contour plot for the primary structure for variation of the damping ratio of the STMD ζ_s under harmonic excitation are illustrated in Figs. 4(a) and 4(b). In order to show the variation of the peak response clearly, a truncated contour plot where the frequency ratio $\omega \in [0.5 \quad 1.5]$ is presented in Fig. 4(b). It is shown in both Figs. 4(a) and 4(b) that the peak response decreases as the damping ratio ζ_s decreases. Figs. 5(a) and 5(b) illustrate the results for variation of damping ratio ζ_s under ground motions where similar conclusions can be drawn.

In order to explain this conclusion, the phase angle θ_p of the primary structure, θ_s of the STMD, and the difference in phase between the structure and the STMD θ_r are presented in Figs. 6(a) - 6(c). Fig. 6(a) indicates that varying the value of the damping ratio ζ_s can change the phase angle of the structure. Decreasing the value of ζ_s is equivalent to increasing the damping ratio of the structure ζ_p because similar result can be obtained for an SDOF structure when increasing its damping ratio (Chopra Anil 2066). Fig. 6(b) illustrates that as the damping ratio ζ_s decreases, the phase angle of the STMD θ_s is approaching π near the resonant frequency, signaling that the STMD oscillates more out of phase with the excitation as ζ_s decreases. In Fig. 6(c), the difference in phase θ_r approaches $\pi/2$ throughout when the damping ratio ζ_s decreases, indicating maximum energy flow and dissipation. It is so because the relative acceleration of the

STMD is in phase with the velocity response of the primary structure. Hence, the power flow is equivalent to an effective dissipative power which increases the total effective damping of the primary structural system. In other words, as ζ_s decreases, the force applied by the STMD to the primary structure is more out of phase to the excitation force $Fe^{i\omega t}$, thereby reducing the structural responses more effectively.

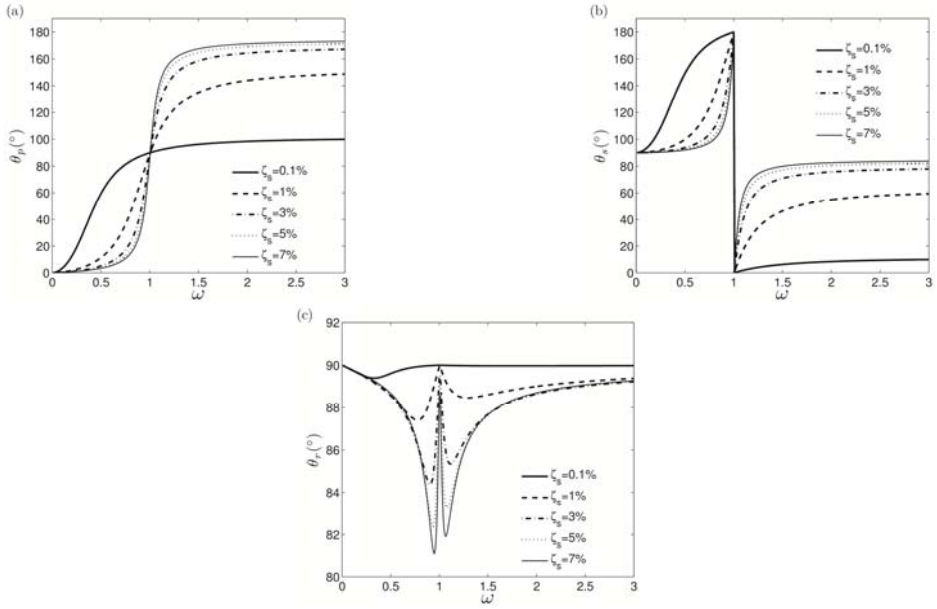

Fig. 6 Phase angle curves for various ζ_s: (a) Phase angle θ_p of the structure; (b) Phase angle θ_s of the STMD and (c) phase angle difference θ_r between the structure and the STMD. Mass ratio $\dot{\alpha}_s = 1\%$

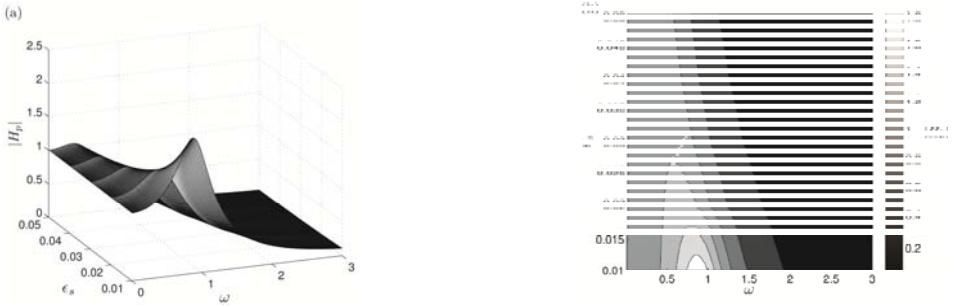

Fig. 7 Structural response with the variation of mass ratio $\dot{\alpha}_s$ under harmonic excitations: (a) frequency response surface and (b) contour plot of the response surface. Damping ratio $\zeta_s = 1\%$

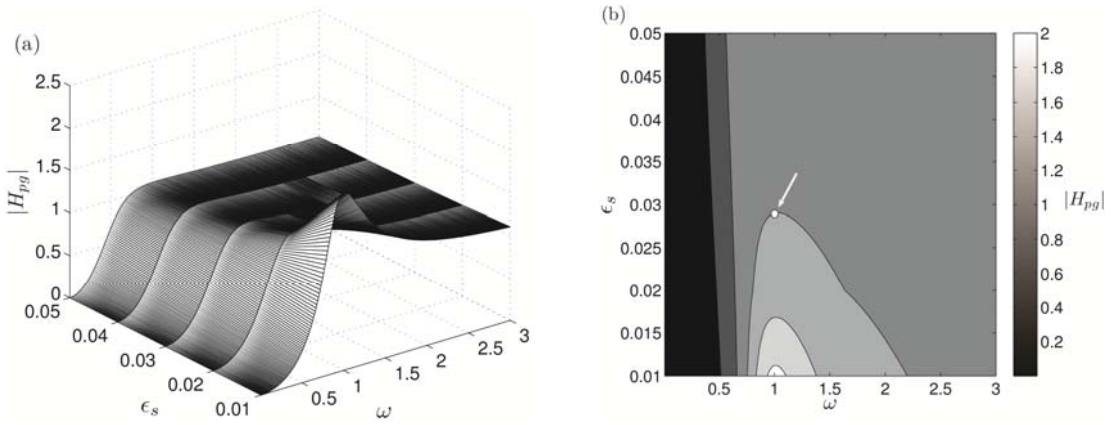

Fig. 8 Structural response with the variation of mass ratio ϵ_s under ground motions: (a) frequency response surface and (b) contour plot of the response surface. Damping ratio $\zeta_s = 1\%$

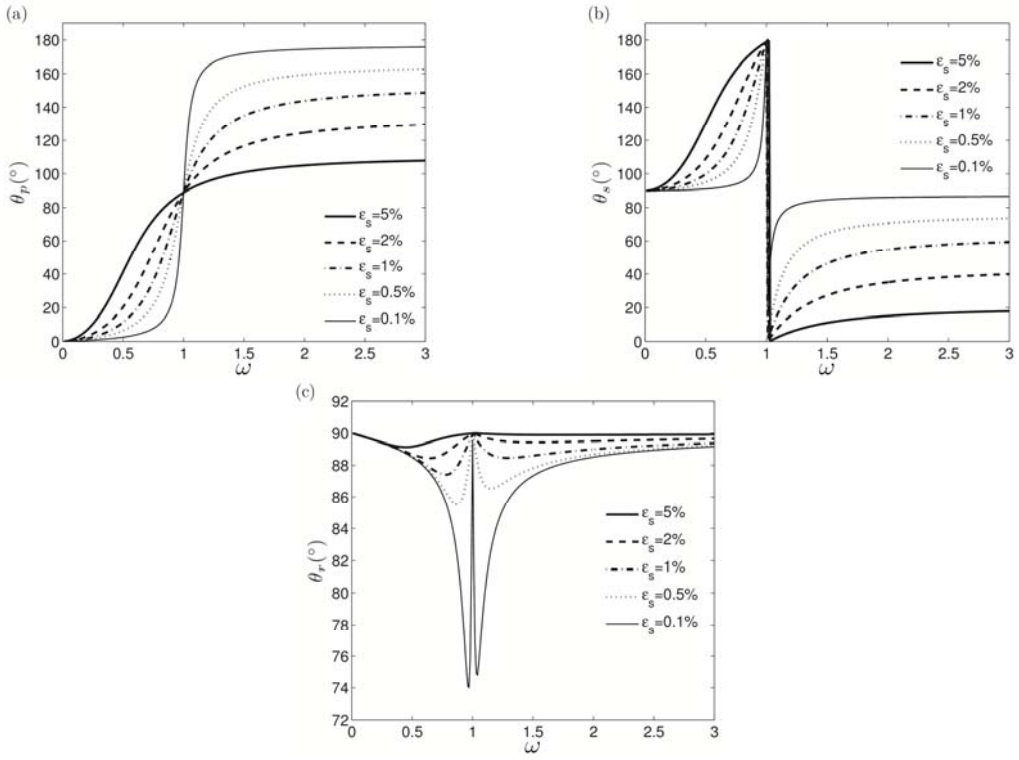

Fig. 9 Phase angle curves for various ϵ_s: (a) Phase angle θ_p of the structure, (b) Phase angle θ_s of the STMD and (c) phase angle difference θ_r between the structure and the STMD. Damping ratio $\zeta_s = 1\%$

4.1.2 Study on STMD mass ratio

Based on the results presented in the previous subsection, $\zeta_s = 1\%$ is adopted in this subsection. Figs. 7(a) and 7(b) illustrate the frequency response surface and the contour plot of the response surface under harmonic excitations as μ is varied. Fig. 7(a) indicates that the peak response decreases as the mass ratio increases; however, little benefit is achieved when increasing μ beyond $\mu = 2.75\%$ as denoted through a bright dot in Fig. 7(b). It is noted that the critical value of the mass ratio $\mu = 2.75\%$ is obtained through sensitivity analysis with respect to the change in the gradient of H_p with respect to μ. Similar analysis is performed to obtain the critical values of μ in other cases.

The results with respect to the variation of the mass ratio under ground motions are shown in Figs. 8(a) and 8(b) where similar conclusions can be drawn as described in Fig. 7. As denoted in Fig. 8(b), the critical value of the mass ratio is $\mu = 3\%$ in the case of harmonic ground motion. The reduction related to the mass ratio μ can also be explained through the variation of the phase angles θ_p, θ_s and θ_r as illustrated in Figs. 9(a) - 9(c).

4.1.3 Sensitivity to frequency mistuning

It is assumed in the previous subsections that the STMD can be tuned exactly to the frequency of the excitation, i.e., $\omega_s / \Omega = 1$. However, there are inevitably small deviations that could occur from data sensing and processing in real world applications. In order to study the effects of the tuning accuracy, a tuning parameter $\beta = \omega_s / \Omega$ is defined. An investigation is performed on the sensitivity of the tuning parameter β. Results for variations of the damping ratio and mass ratio are illustrated in Figs. 10(a) and 10(b). The peak primary structure response is plotted for a range of mistuning levels for different values of μ.

It is shown in Fig. 10(a) where $\mu = 1\%$ that the sensitivity increases when ζ_s decreases. Taking $\zeta_s = 1\%$ as an example, a deviation of 5% off $\beta = 1.0$ causes the peak to increase more than eight times. Similar conclusions can be drawn in Fig. 10(b) where $\mu = 5\%$. In addition, it is observed in Fig. 10 (b) that it is less sensitive when $\beta \le 1.0$ than when $\beta \ge 1.0$. By comparing the case of $\mu = 1\%$ in Fig. 10(a) and that of $\mu = 5\%$ in Fig. 10(b), it is indicated that the performance becomes more robust to the mistuning β as the mass ratio μ increases. It is noteworthy to point out that the results in Fig. 10 are obtained in the case of harmonic excitations. Similar results are obtained in the case of harmonic ground motion which are not shown here due to the limitation of space.

As a summary of this section, it can be concluded that both the mass ratio μ and the damping ratio ζ_s of the STMD can affect the attenuation of the structural response. In order to achieve a satisfactory reduction effect, a small damping ratio ($\zeta_s = 1\%$ is recommended) and an appropriate mass ratio, for example, $\mu = 2.75\%$ in the case of harmonic excitations and $\mu = 3\%$ in the case of ground motions are preferable. In the following sections, the results associated with Model II will be presented and discussed.

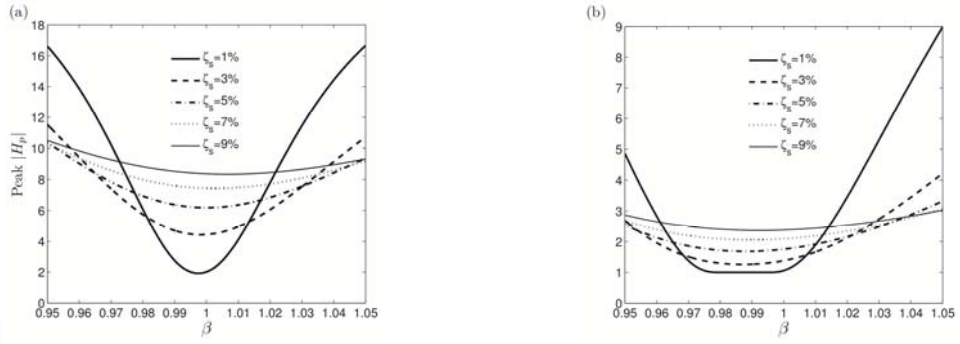

]

Fig. 10 Sensitivity analysis on the tuning parameter β . Mass ratio $\mu_s = 1\%$ in (a) and $\mu_s = 5\%$ in (b)

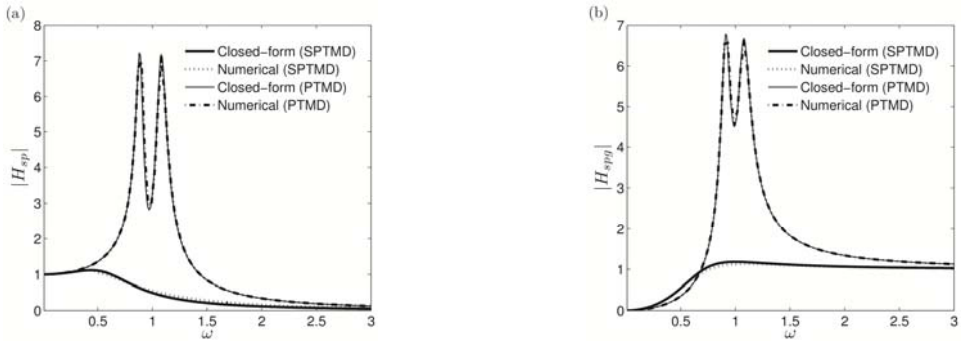

Fig. 11 Verification of the closed-form solution (a) under harmonic loadings and (b) under ground motions. Parameter values: $\mu_s = 3\%$, $\zeta_s = 1\%$, $\zeta_t = 6\%$, $f_t = 0.98$, $F = 0.1$ in (a) and $\zeta_t = 8\%$, $f_t = 0.98$, $X_g = 0.05$ in (b)

4.2. Results of the SPTMD

This section illustrates the results of Model II which is represented by approximate linear ODEs. In order to show the accuracy of the closed-form solutions, numerical results are computed and presented for comparison. In addition, attenuation with respect to the variation of mass ratios and damping ratios are illustrated.

4.2.1. Comparison with numerical results

Fig. 11 illustrate the comparison between the closed-form solutions and the numerical results obtained using numerical integration method. A PTMD is included in the verification. In order to minimize the peak of $|H_{sp}|$ and $|H_{spg}|$ in the case of PTMD, the value of the damping ratio is set to $\zeta_t = 6\%$ in Figs. 11(a) and $\zeta_t = 8\%$ in Fig. 11(b) based on (Gerges *et al*. 2005) the frequency ratio f_t is set to $f_t = 0.98$ in both Figs. 11(a) and 11(b). Fig. 11(a) shows the results under harmonic excitations and Fig. 11(b) shows the case of harmonic ground motion. In Fig. 11(a), it is indicated that the closed-form solution is in good agreement with the numerical result in

the case of the PTMD when the amplitude of the harmonic excitation is relatively small; in the case of the SPTMD, the closed-form solution agrees well with the numerical result despite the slight difference. A similar conclusion can be drawn in Fig. 11(b) in the case of harmonic ground motion.

In order to show the attenuation effectiveness of the SPTMD and the PTMD, magnitude of the transfer function of the primary structure under excitations with no TMD, with PTMD, and with SPTMD are illustrated in Fig. 12.

Fig. 12 indicates that the PTMD can effectively attenuate the structural response; in comparison, the SPTMD can further improve the reduction of the structural responses.

Figs. 13(a) and 13(b) illustrate the frequency response surface and the associated contour plot for variation of the damping ratio ζ_{sp} under harmonic excitation. It is shown in Figs. 13(a) and 13(b) that the peak of the response surface decreases as the damping ratio ζ_{sp} decreases. Similar conclusions can be drawn in the case of ground motions as shown in Figs. 14(a) and 14(b). Actually, the variation of the damping ratio of the SPTMD do influence the phase angle of the primary structure θ_p and also the phase difference θ_r in a similar way described in Fig. 4. Due to the similarities, plots of this data are not shown here.

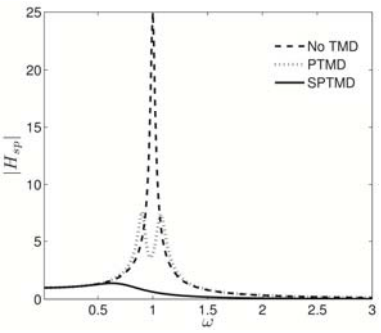

Fig. 12 Frequency response of the cases with no TMD, with a PTMD and with a SPTMD, respectively. Values of parameters: $\zeta_s = 3\%$, $\zeta_{sp} = 1\%$, $\zeta_t = 6\%$, $f_t = 0.98$

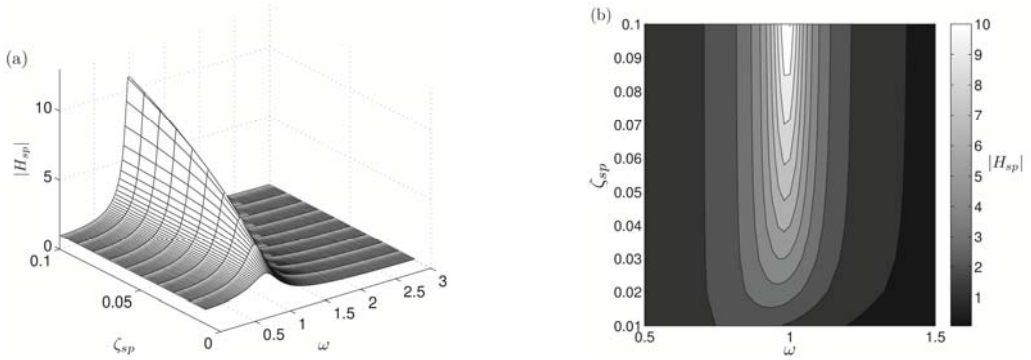

Fig. 13 Frequency response of the primary structure with the variation of the damping ratio ζ_{sp} under harmonic excitations: (a) frequency response surface (b) contour of the response surface. Parameter value: $\zeta_s = 1\%$

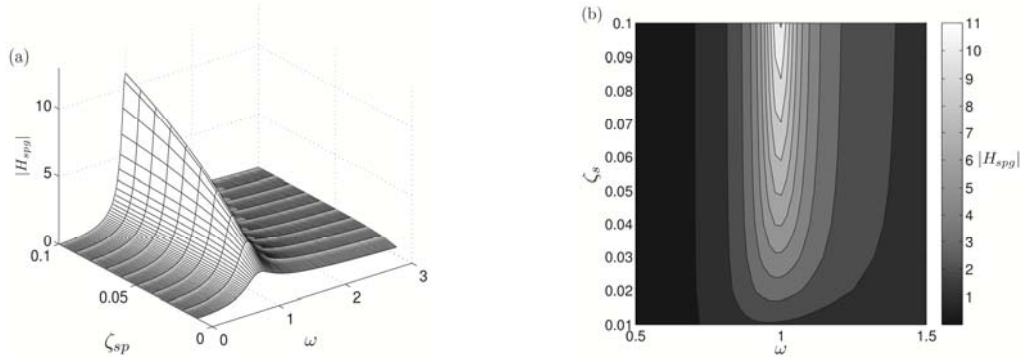

Fig. 14 Frequency response with the variation of damping ratio ζ_{sp} under ground motions: (a) frequency response surface (b) contour of the response surface. Parameter value: $\grave{o}_s = 1\%$

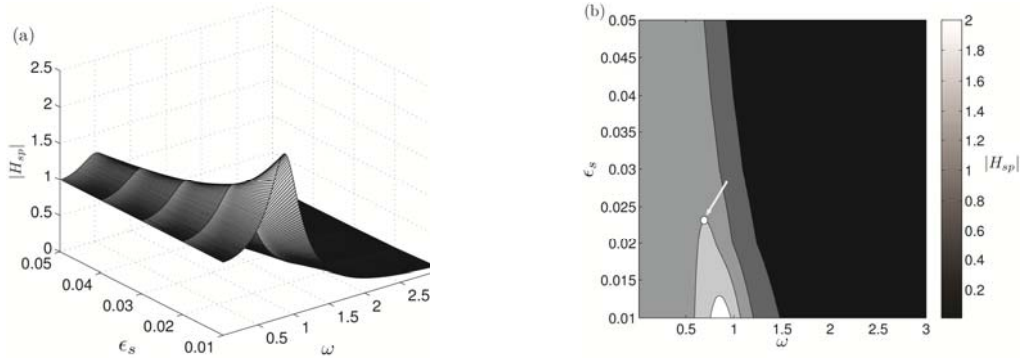

Fig. 15 Frequency response surface of the primary structure with the variation of mass ratio $\grave{o}_s$ under harmonic excitation: (a) frequency response surface (b) contour of the response surface. Parameter value: $\zeta_{sp} = 1\%$

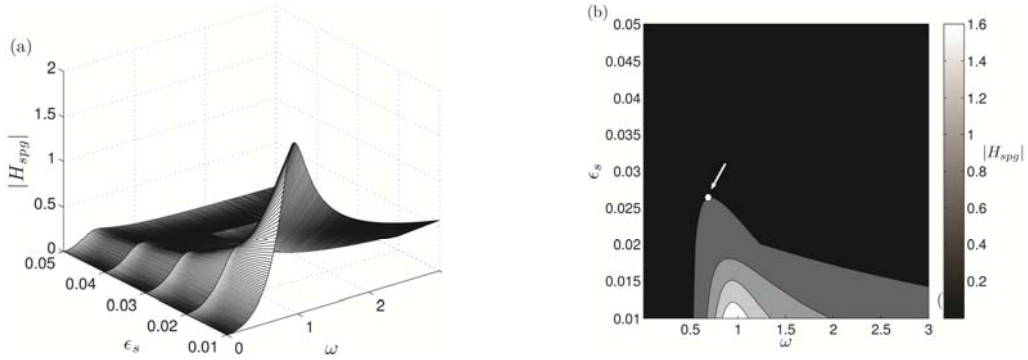

Fig. 16 Frequency response surface of the primary structure with the variation of mass ratio $\grave{o}_s$ under ground motions: (a) frequency response surface (b) contour of the response surface. Parameter value: $\zeta_{sp} = 1\%$

4.2.3 Study on SPTMD mass ratio

Figs. 15(a) and 15(b) show the frequency response surface and the contour plot for variation of the mass ratio μ_s. Fig. 15(a) indicates that the peak of the response surface decreases as the mass ratio μ_s increases.

However, little reduction is produced if μ_s increases after $\mu_s = 3\%$ as denoted through a bright dot. A similar conclusion is obtained from Figs. 16(a) and 16(b) in the case of ground motions.

Sensitivity of the attenuation with respect to the variation of the tuning parameter β is also performed for the SPTMD. Similar conclusions as these discussed in Section 4.1.3 are obtained, i.e., as the mass ratio increases, the attenuation with the PSTMD becomes more robust. Due to the similarities, plots of this data are not shown here.

In order to summarize the results presented in this section, closed-form results show that the SPTMD can produce significant attenuation of the structural responses with appropriate values for the damping ratio and mass ratio. In order to verify the results shown in this section, experimental results are presented in the next section.

5. Experimental verification

This section presents the experimental result for the SPTMD under harmonic ground motion. The scheme and the actual experimental setup of the SPTMD and the primary structure is shown in Fig. 17 where the SPTMD is attached to the top storey. The primary structure is a two degrees-of-freedom system constructed of $1/8 \times 2\ inch$ aluminum columns and $1/2 \times 2\ inch$ steel floors assumed to be rigidly fixed by threaded screw joint connections in a $3:4$ (floor:column) ratio. The system is excited at its base by a shaking table driven by a linear actuator controlled by DSPACE digital hardware and computer input. A laser displacement sensor is placed at the floor levels to capture the system response from base excitation.

Displacement of the top storey and the acceleration of each of the storeys are recorded in the experiment. When the structure reaches steady-state, the length of the SPTMD is adjusted in terms of the feedback frequency tracked with the STFT control algorithm (Nagarajaiah 2009). In addition to the case of a SPTMD, a passive PTMD whose length is not adjusted in real time is used for comparison.

It is identified in the experiment that the frequencies of the two-storey structure are $f_1 = 2.5Hz$ and $f_2 = 7.0Hz$. The two modal damping ratios are $\zeta_1 = 2\%$ for the first mode and $\zeta_2 = 2\%$ for the second mode. The mass ratio is $\mu_s = 0.10$. The frequency of the ground motion is set to $\Omega = 2.5Hz$. Experimental results are shown in Figs. 18 and 19.

Fig. 18(a) illustrates the displacement time history for three cases: no TMD, PTMD, and SPTMD. The pendulum length in the case of the PTMD is initially set to $1.3in$ $(t = 25s)$ when steady-state is reached and finally set to the optimal length $1.5in$ $(t = 50s)$. In the case of the SPTMD, the length is set to $l_s = 1.5in$ $(t = 10s)$ once steady-state is reached. In Fig. 18(a), it is indicated that the real-time tuned SPTMD will significantly reduce the structural response when compared to the case with no TMD and with the PTMD. Fig. 18(b) illustrates that the simulation

results agrees well with the experimental data presented in Fig. 18(a).

Fig. 19(a) shows the transfer function of the acceleration recorded at the top storey in the experiment. It is illustrated in Fig. 19(a) that both the PTMD and the SPTMD can reduce the acceleration of the top floor significantly; in comparison with the PTMD, the SPTMD is more effective. Fig. 19(b) shows the theoretical results calculated from Eq. (25). By comparing Figs. 19(a) and 19(b), it is indicated that the theoretical model can predict the structural responses well.

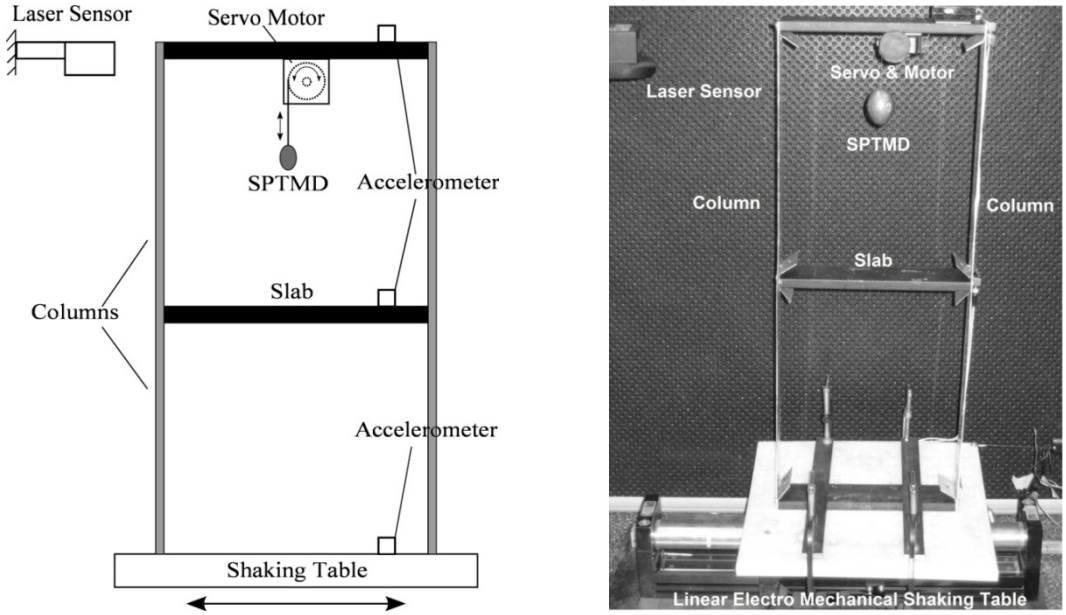

Fig. 17 Experimental setup: (a): Schematic model and (b): actual model

6. Conclusions

This paper studies two types of STMDs with variable frequency properties which are realized by the SAIVS device and a pendulum with an adjustable length. It is found theoretically and experimentally in the present study that the variable frequency smart TMDs (both the SAIVS STMD and the SPTMD) can produce significant reduction of structural responses under harmonic excitations and ground motions. Based on the results presented and discussed in the paper, the following conclusions can be drawn.

1. The closed-form solutions of the dynamic system (Model I and Model II) provide insight into the two degrees-of-freedom system with STMD: the variation of the damping ratio and the mass ratio can affect attenuation through influencing the phase angle of the structure, the phase angle of the STMD, and the phase difference between the structure and the STMDs.
2. Theoretically, a zero damping ratio for the STMD produces the best attenuation; however, $\zeta_s = 1\%$ is recommended to prevent undue sensitivity to tuning parameter β.

3. There exists a critical value of the mass ratio for both Model I and Model II to achieve desirable reduction. When $\zeta_s = 1\%$, the critical value $\dot{o}_s = 2.75\%$ under harmonic excitation and $\dot{o}_s = 3\%$ under harmonic ground motion are preferable for Model I; the value $\dot{o}_s = 2.5\%$ is preferable in the two cases for Model II. As a summary, $\dot{o}_s = 3\%$ is recommended for all the cases.
4. Reduction with the STMD (or SPTMD) is sensitive to the accuracy of the tuning when the mass ratio and the damping ratio are small. However, the robustness to mistuning increases as the mass ratio $\dot{o}_s$ and the damping ratio $\dot{o}_s$ increase.
5. Experimental results agree well with the closed-form results, indicating that the approximate simplification of the equations of motion of Model II is appropriate when the amplitudes of the excitations (or the ground motions) are relatively small.

Further study will investigate the stability of Model II when the nonlinearity of the pendulum is taken into consideration if the pendulum experiences large displacement.

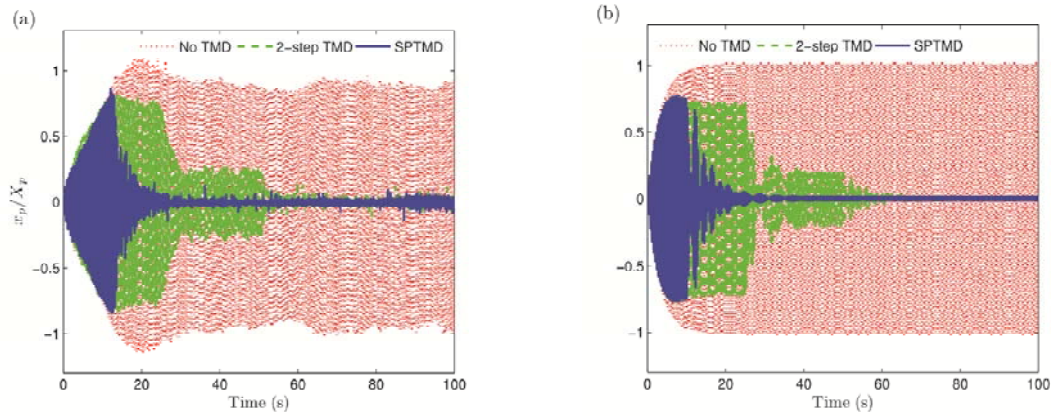

Fig. 18 Displacement time history of the top floor: (a) experimental result and (b) theoretical result. Length of the SPTMD is set to $l_s = 1.5in$ at $t = 10s$; length of the PTMD is set to $l = 1.3in$ at $t = 25s$ and adjusted to $l = 1.5in$ at $t = 50s$

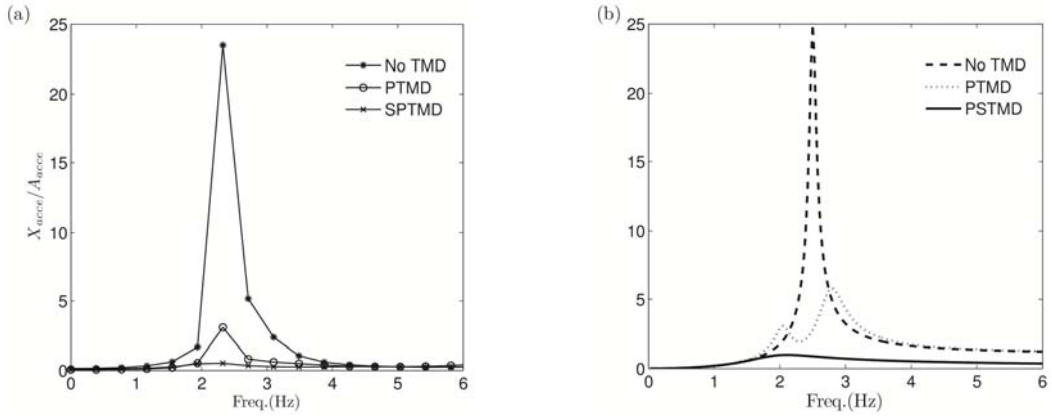

Fig. 19 Acceleration frequency transfer function (a) experimental result and (b) simulation result

References

Abe, M. (1996), "Semi-active tuned mass dampers for seismic protection of civil structures", *Earthq. Eng. Struct. D.*, **25**(7), 743-749.

Abe, M and Igusa, T. (1996), "Semi-active dynamics vibration absorbers for controlling transient response", *J. Sound Vib.*, **198**(5), 547-569.

Chopra Anil K.(2006), *Dynamics of structures:* (3rd Ed.), Prentice Hall.

Den Hartog, J.P. (1956), *Mechanical vibrations* (4th Ed.), McGraw-Hill, New York.

Eason, R.P., Sun, C., Nagarajaiah, S. and Dick, A.J. (2013), "Attenuation of a linear oscillator using a nonlinear and a semi-active tuned mass damper in series", *J. Sound Vib.*, **332**(1), 154-166.

Frahm, H. (1911), *Device for damping vibration of bodies*, US Patent (989,985).

Gerges, R.R. and Vickery, B.J. (2005), "Pendulum tuned mass dampers for floor vibration control", *Struct Des. Tall Spec.*, **14**(4), 353-368.

Housner, G.W., Bergman L.A., Caughey T.K., Chassiakos A.G. and Claus R.O., Masri, S., Skelton, R., Soong, T., Spencer, B., and Yao, J. (1997), "Structural control: past, present, and future", *J. Eng. Mech. - ASCE*, **123**(9), 691-705.

Hrovat, D., Barak, P. and Rabins, M. (1983), "Semi-active versus passive or active tuned mass dampers for structural control", *J. Eng. Mech. - ASCE*, **109**(3), 897-971.

Kobori T., Takahashi M., Nasu T. and Niwa N. (1993), "Seismic response controlled structure with active variable stiffness system", *Earthq. Eng. Struct. D.*, **22**(11), 925-941.

Nagarajaiah, S. and Mate, D. (1998), "Semi-active control of continuously variable stiffness system", *Proceedings of the 2nd World Conference on Structural Control* , Kyoto, Japan.

Nagarajaiah, S. (2000), *Structural vibration damper with continuously variable stiffness*, US Patent No. (6098969).

Nagarajaiah, S. and Varadarajan, N. (2005), "Short time Fourier transform algorithm for wind response control of buildings with variable stiffness TMD", *J. Eng. Struct.*, **27**(3), 431-441.

Nagarajaiah, S. and Sonmez, E. (2007), "Structures with semiactive variable stiffness single/multiple tuned mass dampers", *J. Struct. Eng.*, **133**(1), 67-77.

Nagarajaiah, S. (2009), "Adaptive passive, semi-active, smart tuned mass dampers: identification and control using empirical mode decomposition, Hilbert transform, and short-term Fourier transform", *Struct. Control Health Monit.*, **16**(7-8), 800-841.

Newmark, N.M. and Hall, W.J. (1982), *Earthquake spectra and design*, Earthquake Engineering Research Institute, Berkeley, Calif.

Ormondroyd, J. and Den Hartog, J.P. (1928), "The theory of the dynamic vibration absorber", *T. Am. Soc. Mech. Eng* , **50**, 9-22.

Spencer, B.F. and Nagarajaiah, S. (2003), "State of the art of structural control", *J. Struct. Eng. - ASCE* **129**(7), 845-856.

Sun, C., Eason, R.P., Nagarajaiah, S. and Dick, A.J. (2013), "Hardening Düffing oscillator attenuation using a nonlinear TMD, a semi-active TMD and a multiple TMD", *J. Sound Vib.*, **332**(4), 674-686.

Sun, C. and Nagarajaiah, S. (2013), "Study on semi-active tuned mass damper with variable damping and stiffness under seismic excitations", *Struct. Control Health Monit.*, DOI:10.1002/stc.1620.

Sun, C., Nagarajaiah, S. and Dick, A.J. (2013), "Experimental investigation of vibration attenuation using nonlinear tuned mass damper and pendulum tuned mass damper in parallel", *Nonlinear Dynam.* (under review).

Varadarajan, N. and Nagarajaiah, S. (2004), "Wind response control of building with variable stiffness tuned mass damper using EMD/HT", *J. Eng. Mech.*, **130**(4), 451-458.

Yamada K. and Kobori T. (1995), "Control algorithm for estimating future responses of active variable stiffness structure", *Earthq. Eng. Struct. D.*, **24**(8),1085-1099.

Yamada K., Ritchey J.K., Baxter A.J. and Murray T.M. (2006), "Pendulum tuned mass dampers for floor vibration control", *J. Perform. Constr. Fac.*, **24**(1), 64-73.

Appendix

The kinetic energy T_s and the potential energy V_s of Model I are expressed as

$$T_s = \frac{1}{2} M_p \dot{x}_p^2 + \frac{1}{2} m_s \dot{x}_s^2 \tag{33}$$

$$V_s = \frac{1}{2} k_p x_p^2 + \frac{1}{2} k_s x_s^2 \tag{34}$$

The Lagrangian L_s is

$$L_s = T_s - V_s = \frac{1}{2} M_p \dot{x}_p^2 + \frac{1}{2} m_s \dot{x}_s^2 - \frac{1}{2} k_p x_p^2 - \frac{1}{2} k_s x_s^2 \tag{35}$$

For a non-conservative dynamic system, the Euler-Lagrange equation is represented as

$$\frac{d}{dt}\left(\frac{\partial L}{\partial \dot{q}_i}\right) - \frac{\partial L}{\partial q_i} = Q_i \tag{36}$$

where $q_i, \dot{q}_i$ are the generalized displacement and velocity of the i^{th} degree-of-freedom and Q_i is the corresponding generalized force.

The generalized force of Model II under harmonic excitation is $Q_s = \{Fe^{i\omega\tau} - c_p \dot{x}_p - c_s(\dot{x}_p - \dot{x}_s), -c_s(\dot{x}_s - \dot{x}_p)\}^T$. Substituting Eqs. (33) and (34) into Eqs. (35) and (36) produces the equation of motion of Model I under harmonic excitation as shown in Eq. (1):

For Model II under harmonic excitation, the kinetic energy T and the potential energy V of the system are

$$T = \frac{1}{2} M_p \dot{x}_p^2 + \frac{1}{2} M_p (\dot{x}_p^2 + 2 l_s \dot{x}_p \dot{\phi} cos\phi + \dot{\phi}^2 l_s^2) \tag{37}$$

$$V = \frac{1}{2} K_p x_p^2 + mgl_s(1 - cos\phi) \tag{38}$$

The Lagrangian L_s is

$$L = T - V = \frac{1}{2} M_p \dot{x}_p^2 + \frac{1}{2} M_p (\dot{x}_p^2 + 2 l_s \dot{x}_p \dot{\phi} cos\phi + \dot{\phi}^2 l_s^2) - \frac{1}{2} K_p x_p^2 - mgl_s(1 - cos\phi) \tag{39}$$

The generalized force of Model II under harmonic excitation is $Q = \{Fe^{i\omega\tau} - c_p \dot{x}_p - c_s(\dot{x}_p - \dot{x}_s), -c_s(\dot{x}_s - \dot{x}_p)\}^T$. Substituting Eq. (39) into Eq. (36) yields the equations of motion of Model II under harmonic excitation as illustrated in Eq. (17)

Parameters c_p, d_p, c_s, d_s in the present paper are

$$\begin{aligned} c_p &= \frac{C_p}{D}, \qquad d_p = \frac{D_p}{D} \\ c_s &= \frac{C_s}{D}, \qquad d_s = \frac{D_s}{D} \end{aligned} \tag{40}$$

The expressions of C_p, D_p, C_s, D_s are listed as follows

$$C_p = -\omega^6 + \omega^4 + (2+\varepsilon_s)\omega^4\Omega_s^2 - 2\omega^2\Omega_s^2 - (1+\varepsilon_s)\omega^2\Omega_s^4 + \Omega_s^4 + 4\varepsilon_s\omega^3\Omega_s^3\zeta_s - 4\varepsilon_s\omega\Omega_s^5\zeta_s - 4(1-\varepsilon_s)\omega^4\Omega_s^2\zeta_s^2 + 4\omega^2\Omega_s^2\zeta_s^2 \tag{41}$$

$$D_p = -2\omega^5\zeta_1 + 4\omega^3\Omega_s^2\zeta_1 - 2\omega\Omega_s^4\zeta_1 - 2\varepsilon_s\omega^5\Omega_s\zeta_s + 4\varepsilon_s\omega^3\Omega_s^3\zeta_s - 4\varepsilon_s\omega\Omega_s^5\zeta_s - 8\varepsilon_s\omega^2\Omega_s^4\zeta_s^2 - 8\omega^3\Omega_s^2\zeta_p\zeta_s^2 - 16\varepsilon_s\omega^3\Omega_s^3\zeta_s^3 \tag{42}$$

$$C_s = \varepsilon_s(\omega^4\Omega_s^2 - \omega^2\Omega_s^2 - \omega^2\Omega_s^4 - \varepsilon_s\omega^2\Omega_s^4 + \Omega_s^4 + 2\omega^5\Omega_s\zeta_s - 2\omega^3\Omega_s\zeta_s - 2\omega^3\Omega_s^3\zeta_s - 2\varepsilon_s\omega^3\Omega_s^3\zeta_s + 2\omega\Omega_s^3\zeta_s - 4\varepsilon_s\omega\Omega_s^5\zeta_s - 4\omega^2\Omega_s^3\zeta_p\zeta_s - 16\varepsilon_s\omega^2\Omega_s^4\zeta_s^2 - 8\omega^3\Omega_s^2\zeta_p\zeta_s^2 - 16\varepsilon_s\omega^3\Omega_s^3\zeta_s^3) \tag{43}$$

$$D_s = \varepsilon_s(2\omega^3\Omega_s^2\zeta_p - 2\omega\Omega_s^4\zeta_p + 2\omega^3\Omega_s^3\zeta_s + 2\varepsilon_s\omega^3\Omega_s^3\zeta_s - 2\omega\Omega_s^3\zeta_s - 4\varepsilon_s\omega\Omega_s^5\zeta_s + 4\omega^4\Omega_s\zeta_p\zeta_s - 4\omega^2\Omega_s^3\zeta_p\zeta_s + 4\omega^4\Omega_s^2\zeta_s^2 + 4\varepsilon_s\omega^4\Omega_s^2\zeta_s^2 - 4\omega^2\Omega_s^2\zeta_s^2 - 8\varepsilon_s\omega^2\Omega_s^4\zeta_s^2) \tag{44}$$

$$D = [(2\omega\Omega_s)(-\omega^2 + 1 + \varepsilon_s\Omega_s^2)\zeta_s + (-\omega^2 + \Omega_s^2)(2\omega\zeta_p + 2\varepsilon_s\omega\Omega_s\zeta_s)]^2 + [(-\omega^2 + \Omega_s^2)(-\omega^2 + 1 + \varepsilon_s\Omega_s^2) - \varepsilon_s\Omega_s^2(\Omega_s + 2\omega\zeta_s)^2 - 2\omega\Omega_s\zeta_s(2\omega\zeta_p + 2\varepsilon_s\omega\Omega_s\zeta_s)]^2 \tag{45}$$